# Hybrid simulations of $m/n = 1/1$ instability driven by energetic counter-passing particles in tokamak plasmas

**Jixing Yang [1], Guoyong Fu [2],†, Wei Shen[3] and MinYou Ye[1],†**

[1]School of Nuclear Science and Technology, University of Science and Technology of China, Hefei 230026, PR China

[2]Institute for Fusion Theory and Simulation and College of Physics, Zhejiang University, Hangzhou 310027, PR China

[3]Institute of Plasma Physics, Chinese Academy of Science, Hefei 230021, PR China

A systematic simulation study of the $n/m = 1/1$ instability driven by energetic counter-passing particles in tokamak plasmas has been carried out using the kinetic-MHD (Magnetohydrodynamics) hybrid code M3D-K. The safety factor's radial profile is monotonically increasing with central value $q_0$ less than unity. The linear simulation results show that the instability is either a $m/n = 1/1$ energetic particle mode or a $m/n = 1/1$ global Alfvén eigenmode depending on the value of the central safety factor. The mode frequencies are close to the tip of Alfvén continuum spectrum at the magnetic axis. The excited modes are radially localized near the magnetic axis well within the safety factor $q = 1$ surface. The main wave particle resonance is found to be $\omega_\phi + 2\omega_\theta = \omega$, where $\omega$ is the mode frequency. The nonlinear simulation results show that there is a long period of quasi-steady-state saturation phase with frequency chirping up after initial saturation. Correspondingly, the energetic particle distribution with low energies is flattened in the core of the plasma. After this quasi-steady phase, the mode amplitude grows again and frequency jumps down to a low value corresponding to a new mode similar to the energetic co-passing particle-driven low-frequency fishbone while the energetic particle distribution is flattened for higher energies in the core of plasma.

Key words: fusion plasma, plasma instabilities, plasma simulation

## 1. Introduction

In the study of magnetically confined fusion plasmas, energetic particle physics is a very important subject (Heidbrink 2008; Gorelenkov, Pinches & Toi 2014; Chen & Zonca 2016). Energetic particles come from auxiliary heatings such as neutral beam injection (NBI) or ion cyclotron resonance heating. Energetic particles are also produced from fusion reactions (i.e. alpha particles) in burning plasmas. Energetic particles can excite various instabilities such as Alfvén eigenmodes, fishbone modes (McGuire *et al.* 1983; Chen, White & Rosenbluth 1984; Coppi & Porcelli 1986; Betti & Freidberg 1993;

† Email addresses for correspondence: gyfu@zju.edu.cn, yemy@ustc.edu.cn

Wang 2001; Yu *et al.* 2019) and energetic particle modes (EPM) (Chen 1994). These instabilities can lead to redistribution and losses of energetic particles. As a consequence, these instabilities may degrade energetic particle heating and even damage the first wall of a fusion reactor. Therefore, it is important to investigate the physics of the energetic particle-driven instabilities in tokamak plasmas.

In this work we focus on the energetic counter-passing particle-driven $n = 1$ mode in tokamak plasmas. Here, $n$ is the toroidal mode number. The prefix counter- denotes the direction of beam ion injection opposite to that of the plasma current. The prefix co- in context means that the direction of beam ion injection is the same as that of the plasma current. The case of the energetic co-passing particle-driven $n = 1$ mode has been investigated in our recent simulation study (Yang *et al.* 2022). It is well known that energetic trapped particles can excite the $m/n = 1/1$ fishbone instabilities in a tokamak plasma with a monotonic safety factor $q$ profile and the central $q$ value less than unity (McGuire *et al.* 1983; Chen *et al.* 1984; Coppi & Porcelli 1986). Here, $m$ is the poloidal mode number. The fishbone can be intrinsically an EPM with a mode frequency comparable to the processional drift frequency $\omega_{d,h}$ of energetic trapped particles (Chen *et al.* 1984). The fishbone can be excited when the energetic particle density exceeds a threshold. On the other hand, there is also another type of fishbone whose mode frequency is comparable to the diamagnetic drift frequency $\omega_{*,i}$ of thermal ions. This fishbone instability, the so-called $\omega_{*,i}$ branch, can also be resonantly destabilized by energetic trapped particles (Coppi & Porcelli 1986). Further work had shown that energetic passing particles can also excite fishbone instabilities (Betti & Freidberg 1993; Wang 2001). Betti *et al.* found that the low-frequency $\omega_{*,i}$ fishbone can be destabilized by passing energetic particles when the effects of finite orbit width of the energetic particles is taken into account (Betti & Freidberg 1993). The corresponding wave particle resonance is $\omega = k_{\parallel} v_{\parallel}$ with $k_{\parallel} \sim (n - m/q)/R$ being the parallel wavenumber with $(n, m) = (1, 1)$ and here $R$ is the major radius. More recently, Yu *et al.* showed analytically that an EPM branch of the low-frequency fishbone can also be destabilized by energetic passing particles with mode frequency determined by the wave particle resonance $\omega = k_{\parallel} v_{\parallel}$ when $\omega_{*,i}$ is neglected (Yu *et al.* 2019). The main conclusions of Yu's work have been confirmed qualitatively by our recent simulation study where the numerical results show that energetic co-passing particles can excite a low-frequency fishbone instability with mode frequency similar to the analytic result (Yang *et al.* 2022). Finally, it was shown earlier that energetic co-passing particles can excite an $n = 1$ high-frequency fishbone of EPM type at a much higher mode frequency (Wang 2001).

In this work, we extend our recent simulation study (Yang *et al.* 2022) of the energetic co-passing particle-driven $n = 1$ mode to the case of the energetic counter-passing particle-driven $n = 1$ mode in tokamak plasmas. The simulations have been carried out using the global kinetic-MHD (Magnetohydrodynamics) hybrid simulation code M3D-K (Fu *et al.* 2006). We consider tokamak parameters similar to those of the HL-2A experiments excepting the direction of neutral beam injection. The $q$ profile is monotonically increasing with radius with its central value $q_0 < 1$. A systematic linear simulation study of key parameter dependences has been carried out. Parameter values of safety factor $q_0$, beam ion beta, beam ion injection energy and thermal plasma beta are scanned. Our linear simulation results show that the beam ion-driven modes are either EPMs or global Alfvén eigenmodes (GAEs) (Appert *et al.* 1982; Mahajan, Ross & Chen 1983). The mode frequencies are much higher than those of the low-frequency fishbone (Betti & Freidberg 1993; Yu *et al.* 2019). The main wave particle resonance driving the instability is identified as $\omega_{\phi} + 2\omega_{\theta} = \omega$, where $\omega_{\theta}$ is the poloidal transit frequency and $\omega_{\phi}$ is the toroidal transit frequency of energetic particles. The nonlinear simulation results
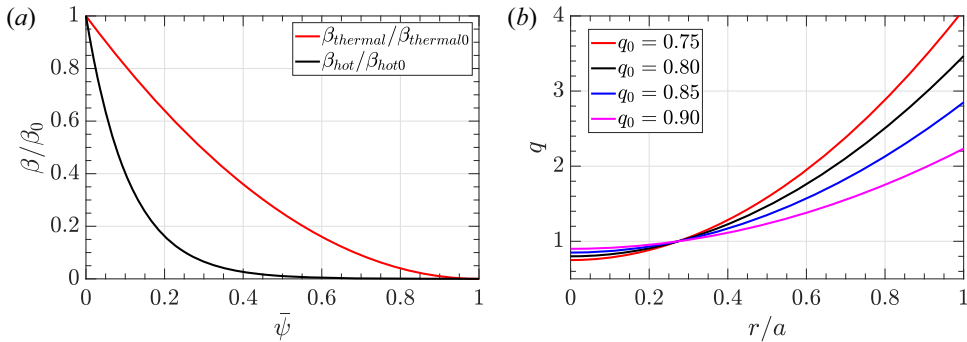
FIGURE 1. (*a*) The $\beta$ profiles and (*b*) safety factor profiles.

show initial mode saturation, a long quasi-steady saturation phase with upward frequency chirping, and finally a second growth phase with frequency jumping down to a lower value. Details of the results will be shown in § 3 and § 4.

This article is organized as follows: § 2 gives a brief introduction to the M3D-K code and parameters and profiles used in our simulation study. In § 3, linear simulation results of the energetic counter-passing particle-driven $n = 1$ mode are presented. Section 4 gives the corresponding nonlinear simulation results of the $n = 1$ mode. Finally, a summary of this work is given in § 5.

## 2. Simulation model and parameter set-up

In this work, we use the global kinetic-MHD hybrid code M3D-K (Fu *et al.* 2006), in which a particle/MHD hybrid model is used to describe the interaction of energetic particles and MHD modes. In this model, the thermal plasma is treated as a single fluid while the energetic particles are described by the drift-kinetic equation. The drift-kinetic equation is solved by the particle-in-cell method (Fu *et al.* 2006). The M3D-K code has been successfully applied to study energetic particle-driven instabilities such as fishbone and energetic particle effects on MHD modes (Fu *et al.* 2006; Lang, Fu & Chen 2010; Cai & Fu 2012; Wang *et al.* 2013; Liu *et al.* 2015; Shen *et al.* 2015, 2017; Zhu, Wang & Wang 2020).

In our simulations, parameters and profiles similar to those of HL-2A tokamak plasmas are used excepting the direction of neutral beam injection. In this work we consider counter-injection beam ions. The main parameters include the major radius $R_0 = 1.6$ m, minor radius $a = 0.4$ m, magnetic field $B_0 = 1.34$ T, central electron density $n_{e0} = 1.3 \times 10^{19}$ m$^{-3}$, Alfvén speed $v_A = B_0/\sqrt{\mu_0 \rho_0} = 5.56 \times 10^6$ ms$^{-1}$, Alfvén time $\tau_A = R_0/v_A = 2.88 \times 10^{-7}$ s and Alfvén frequency $\omega_A = 1/\tau_A = 3.7 \times 10^6$ s$^{-1}$. Both the thermal ion species and energetic ion species are deuterium ions. The thermal plasma and energetic particle beta profile are, respectively, $\beta_{\mathrm{thermal}} = \beta_{\mathrm{thermal0}}(1 - \bar{\psi})^2$ and $\beta_{\mathrm{hot}} = \beta_{\mathrm{hot0}} \exp(-\bar{\psi}/0.11)$, where $\bar{\psi} = (\psi - \psi_{\mathrm{min}})/(\psi_{\mathrm{max}} - \psi_{\mathrm{min}})$ is the normalized poloidal magnetic flux varying from $\bar{\psi} = 0$ at the magnetic axis to $\bar{\psi} = 1$ at the edge of plasma. Figure 1(*a*) shows these two normalized profiles. The $q$ profile is given by $q = c_1 + c_2(r/a)^2$, where $c_1$ equals the safety factor value at the magnetic axis $q_0$ and $c_2$ is adjusted to fix the radius $r|_{q=1} = 0.274a$ of the $q = 1$ surface. Here, $r^2/a^2 = \bar{\phi}$, where $\bar{\phi}$ is the normalized toroidal flux. Figure 1(*b*) shows the $q$ profiles with $q_0$ equal to 0.75, 0.80, 0.85 and 0.90.

For the energetic beam ions, a slowing-down distribution in velocity is used along with a peaked distribution in pitch angle for deeply counter-passing particles. The beam ion

distribution $F$ is given by

$$F = c_n n_0 F_1 \left( \langle \bar{\psi} \rangle \right) F_2 (v) F_3 (\Lambda), \tag{2.1}$$

where $c_n$ is an overall normalization coefficient, $n_0$ is the central density, $F_1(\langle \bar{\psi} \rangle)$, $F_2(v)$ and $F_3(\Lambda)$ are the distribution in space, velocity $v$ and pitch angle parameter $\Lambda$, respectively. Here, $\Lambda = \mu B_0 / E$, with $\mu$ being the magnetic moment and $E$ being the energy; $F_1(\langle \bar{\psi} \rangle)$ is given by

$$F_1 \left( \langle \bar{\psi} \rangle \right) = \exp \left( -\frac{\langle \bar{\psi} \rangle}{\Delta \bar{\psi}} \right), \tag{2.2}$$

where $\langle \bar{\psi} \rangle$ is the normalized orbit-averaged value of poloidal flux defined by $\langle \bar{\psi} \rangle = (P_\phi - m \langle v_\parallel R B_\phi / B \rangle) / [e(\psi_{max} - \psi_{min})] - \psi_{min} / (\psi_{max} - \psi_{min})$, with $P_\phi$ being the toroidal canonical angular momentum. Also, $\Delta \bar{\psi} = 0.11$ is the width of radial profile and $F_2(v)$ is given by

$$F_2 (v) = \frac{1}{2 \left( v^3 + v_c^3 \right)} \left[ 1 + \mathrm{erf} \left( \frac{v_0 - v}{\Delta v} \right) \right], \tag{2.3}$$

where $v_0$ is the injection speed of the NBI, $v_c = (0.75 \sqrt{\pi} m_e / m_i)^{1/3} v_{Te}$ is the critical velocity and $v_c$ is chosen to be a constant for simplicity and is given by $v_c = 0.6 v_0$ in this simulation work. Also, $\Delta v = 0.1 v_0$ is the width of the distribution around the injection speed, erf is the error function and $F_3(\Lambda)$ is given by

$$F_3 (\Lambda) = \frac{2}{\sqrt{\pi} \Delta \Lambda} \frac{1}{\mathrm{erf} \left( \dfrac{1 - \Lambda_0}{\Delta \Lambda} \right) + \mathrm{erf} \left( \dfrac{\Lambda_0}{\Delta \Lambda} \right)} \exp \left[ - \left( \frac{\Lambda - \Lambda_0}{\Delta \Lambda} \right)^2 \right], \tag{2.4}$$

where $\Lambda_0 = 0.0$ is the central pitch angle parameter and $\Delta \Lambda = 0.2$ is the width of pitch angle distribution.

## 3. Linear simulation results

In this section we present the linear simulation results of the $n = 1$ mode driven by energetic counter-passing beam ions. Key beam ion parameters of injection energy $E_0$, particle beta as well as safety factor profile and thermal plasma beta are varied in our simulation study in order to investigate the dependence of the instability on these key parameters.

### 3.1. *The simulation results of the baseline case with $q_0 = 0.85$, $E_0 = 60$ keV*

Here, we present the baseline simulation case with parameters $q_0 = 0.85$, $E_0 = 60$ keV. Figures 2(*a*) and 2(*b*) show the mode structures of the streamfunction $U$ without and with beam ions, respectively. Here, $U$ is the streamfunction of the incompressible part of the plasma velocity. Without beam ions, $\beta_{thermal0} = 1.3\%$, $\beta_{hot0} = 0\%$, the mode is a typical internal kink mode. With the beam ions, $\beta_{thermal0} = 0.01\%$, $\beta_{hot0} = 1.3\%$, a mode localized near the magnetic axis with a narrow radial structure is excited. The mode has the poloidal mode number $m = 1$ and toroidal mode number $n = 1$. To identify the type of the mode, figure 2(*c*) plots the continuum spectrum of $m/n = 1/1$ for $q_0 = 0.85$. The dashed blue line represents the frequency of the baseline case. The frequency is close to the tip of the continuum at the magnetic axis and has an intersection with the continuum
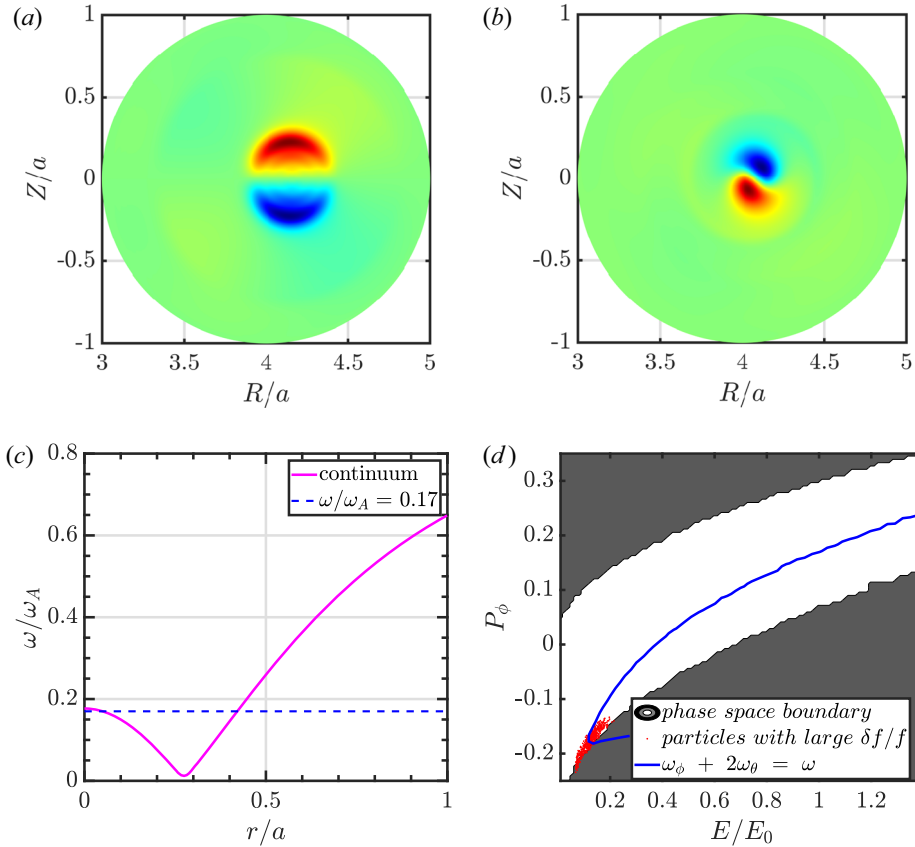
FIGURE 2. The results of the baseline case: (*a*) the internal kink mode structure (contour of $U$), (*b*) the EPM mode structure (contour of $U$), (*c*) the continuum and (*d*) the resonance condition.

line. Therefore, this mode is identified as EPM. It should be pointed out that the value of the thermal beta is chosen to be very small for simplicity for most of our results. We will show later that the effects of finite thermal beta do not change much the characters of the modes found.

Now we consider the main wave particle resonance responsible for driving the mode. In general, the wave particle resonant condition is given by (Porcelli *et al.* 1994)

$$n\omega_\phi + p\omega_\theta = \omega, \tag{3.1}$$

where $n$ is the toroidal mode number ($n = 1$ in this study), $p$ is an integer denoting the poloidal harmonic, $\omega$ is the mode frequency, $\omega_\theta \equiv \Delta\theta/\Delta t$ is the poloidal transit frequency of beam ions and $\omega_\phi \equiv \Delta\phi/\Delta t$ is the toroidal transit frequency.

In order to identify the main wave particle resonance, we plot the locations of simulation particles with the largest values of particle weight $w = \delta f/f$ in the phase space of $(P_\phi, E)$, where $\delta f$ is the perturbed distribution function of energetic beam ions. In the phase space, energetic particles lie in the white area rather than the grey area. It is known that resonant particles usually have the largest values of particle weight because of the secular change of the perturbed distribution function at resonances. Figure 2(*d*) shows that resonant particles (circles) are located on the $p = 2$ resonance line (solid line). This result indicates that the main wave particle resonance is $\omega_\phi + 2\omega_\theta = \omega$. It should be pointed out that, in this study,
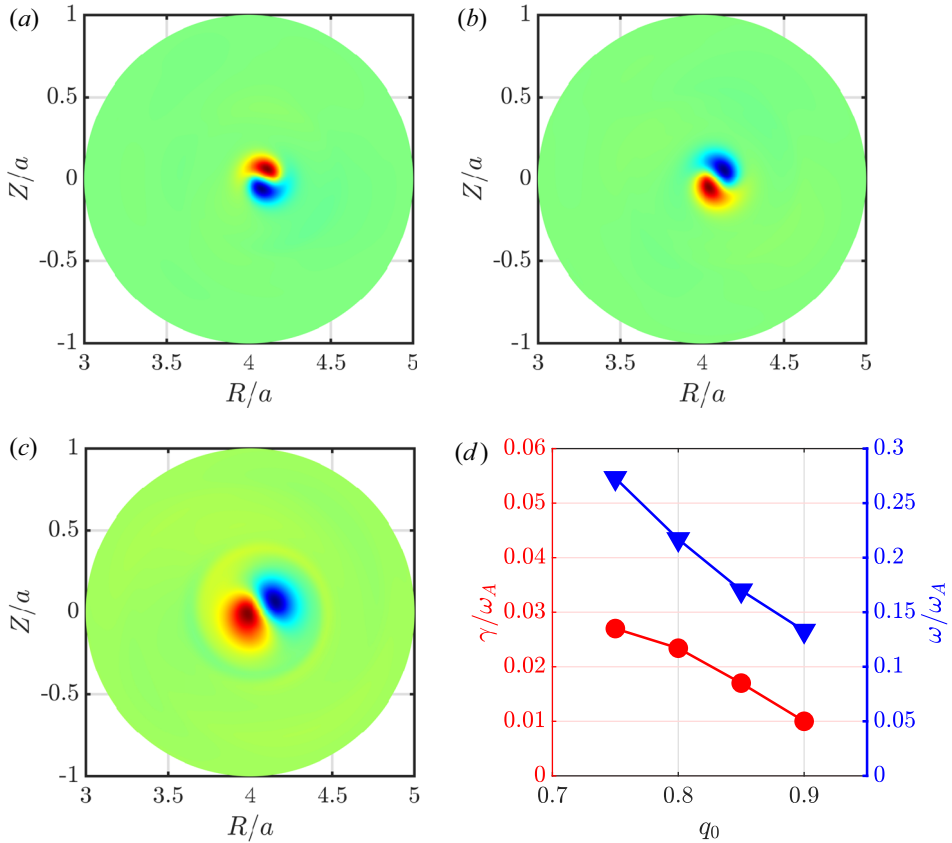
FIGURE 3. The mode structure (contour of $U$) of cases with (a) $q_0 = 0.75$, (b) $q_0 = 0.80$ and (c) $q_0 = 0.90$; (d) the growth rate and frequency as the function of $q_0$.

the beam ions are counter-passing particles with positive $\omega_\phi$ and negative $\omega_\theta$ in the M3D-K code convention. Furthermore, the simulated mode frequency $\omega$ is negative, indicating that the mode rotates toroidally in the direction of the plasma current or in the ion diamagnetic direction.

### 3.2. *The dependence on* $q_0$

In this section, the $q$ profile is scanned while keeping the other parameters the same as in the baseline case. Figures 3(a), 3(b) and 3(c) show the mode structures with $q_0 = 0.75$, $q_0 = 0.80$ and $q_0 = 0.90$, respectively. It can be seen that, as $q_0$ increases, the mode structure becomes broader. Figure 3(d) shows the simulation results of growth rate (red line) and mode frequency (blue line) as a function of $q_0$. As $q_0$ rises, the growth rate and the frequency decrease. All these four cases have the same dominating resonance $\omega_\phi + 2\omega_\theta = \omega$ as shown in figure 4. It can be found that the resonant particles of the $q_0 = 0.75$ case (figure 4a) have larger energies than those of the $q_0 = 0.90$ case (figure 4b). This is why the cases with smaller $q_0$ have larger growth rates than the cases with larger $q_0$.

Figures 5(a) and 5(b) show the continuum spectrum of $m/n = 1/1$ for $q_0 = 0.75$ and $q_0 = 0.90$, respectively. The dashed blue lines represent the frequencies of the corresponding cases. The frequency of the $q_0 = 0.75$ case intersects with the continuum line near the magnetic axis. Therefore, this mode is also an EPM. It should be pointed
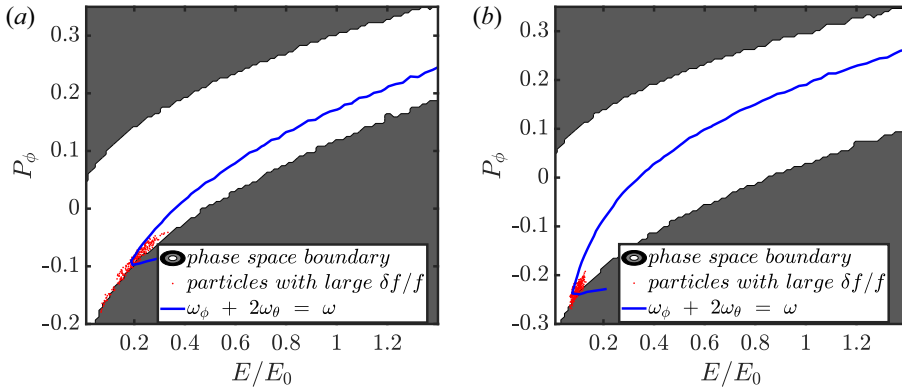
FIGURE 4. The resonance condition of cases with (*a*) $q_0 = 0.75$ and (*b*) $q_0 = 0.90$.
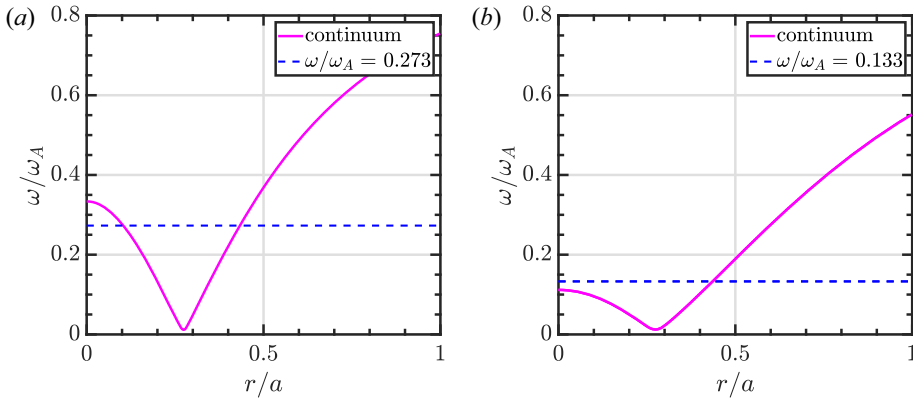


FIGURE 5. Continuum spectrum of cases with (*a*) $q_0 = 0.75$ and (*b*) $q_0 = 0.90$.

out that the mode of the $q_0 = 0.80$ case is also an EPM. The frequency of the $q_0 = 0.90$ case is higher than the tip of the continuum at the magnetic axis. Therefore, the mode in this case is identified as GAE (Appert *et al.* 1982). The corresponding mode structure is typically broader than those of EPM, as shown in figure 3(*c*). The GAE was first found by Appert *et al.* (1982). The mode typically exists with its frequency slight below the minimum of the Alfvén continuum in a cylindrical geometry. Sometime GAE can exist above the maximum of the Alfvén continuum due to effects of toroidicity and/or energetic particles. Here, the GAE is found to be localized near the magnetic axis with its frequency slight above the maximum of the Alfvén continuum at the magnetic axis.

To summarize, mode features are sensitive to $q_0$. As $q_0$ increases from 0.75 to 0.90, the mode frequency decreases and the mode type changes from EPM to GAE.

### 3.3. *The dependence on beam ion beta*

In this subsection, we scan beam ion beta with fixed $q_0 = 0.80$ and $q_0 = 0.90$. We choose $\beta_{\text{thermal0}} = 0.01\,\%$ and $E_0 = 60\,\text{keV}$. Figure 6(*a*) shows the growth rate and frequency as a function of beam ion beta for $q_0 = 0.80$. It can be seen that there exists a critical beta of $0.76\,\%$ above which the EPM is unstable. The frequency is not sensitive to $\beta_{\text{hot0}}$. Figure 6(*b*) shows the growth rate and frequency as a function of beam ion beta for $q_0 = 0.90$. It can be seen that there also exists a critical beta of $1.16\,\%$. The frequency
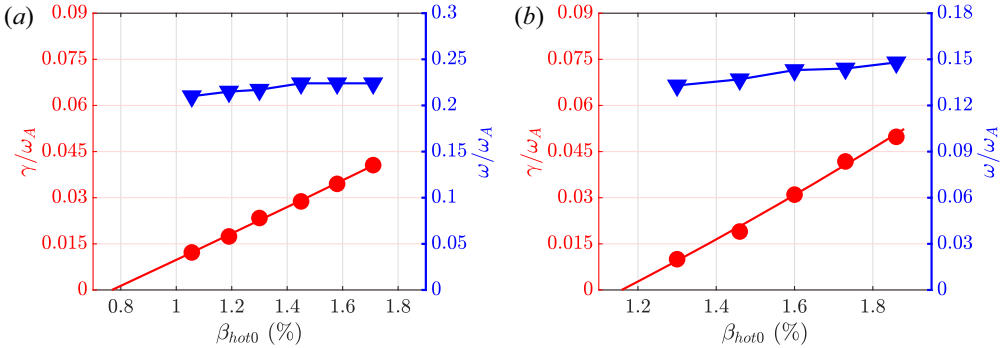
FIGURE 6. Growth rate and frequency dependence on $\beta_{\text{hot0}}$ for (a) $q_0 = 0.80$, (b) $q_0 = 0.90$.

is also not sensitive to $\beta_{\text{hot0}}$. Furthermore, it is found that the mode character does not change much as the beam ion beta varies. For the case with $q_0 = 0.80$, the destabilized modes are all EPMs. On the other hand, for the case of $q_0 = 0.90$, the destabilized modes are all GAEs. The main resonances of all these cases are the same as in the baseline case, i.e. $\omega_\phi + 2\omega_\theta = \omega$.

To summarize the results of this subsection, both mode structures and mode frequencies are not sensitive to the beam ion beta. There exists a critical beam ion beta above which the mode is destabilized for both EPM and GAE.

### 3.4. *The dependence on $E_0$*

In this subsection, we investigate the dependence of the beam ion-driven $n = 1$ modes on beam ion injection energy $E_0$. For the case of EPM with $q_0 = 0.80$, we choose beta values of $\beta_{\text{hot0}} = 1.3\,\%$ and $\beta_{\text{thermal0}} = 0.01\,\%$. For the case of GAE with $q_0 = 0.90$, we choose beta values of $\beta_{\text{hot0}} = 1.6\,\%$ and $\beta_{\text{thermal0}} = 0.01\,\%$. Figures 7(a) and 7(b) show the simulation results of growth rate (red line) and mode frequency (blue line) as a function of $E_0$ for $q_0 = 0.80$ and $q_0 = 0.90$, respectively. It can be seen that the growth rate of both EPM and GAE decrease as $E_0$ increases. The frequencies of these two modes are not sensitive to $E_0$. Figures 8(a) and 8(b) give the mode structures of $q_0 = 0.80$ (EPM) with $E_0 = 30$ and $75\,\text{keV}$, respectively. We observe that the mode structures are similar. Figures 8(c) and 8(d) show the corresponding resonance locations of these two cases. It can be seen that, as $E_0$ rises, the area in which the resonant particles are located moves father away from $E_0$ in phase space. It should be noted that the strength of wave particle resonant interaction with respect to energetic particle drive decreases as the normalized resonant energy $E_{res}/E_0$ becomes smaller. This explains why the growth rate decreases as $E_0$ increases, as shown in figure 7.

To summarize this subsection, the mode frequencies of both EPM and GAE are not sensitive to beam ion injection energy $E_0$ while the growth rates decrease as $E_0$ increases.

### 3.5. *The dependence on thermal ion beta*

In this subsection, we scan thermal plasma beta with fixed $q$ values of $q_0 = 0.80$ and $q_0 = 0.90$. We choose $E_0 = 60\,\text{keV}$. For the $q_0 = 0.80$ cases, we choose a beam ion beta of $\beta_{\text{hot0}} = 1.0\,\%$. For the $q_0 = 0.90$ cases, we choose $\beta_{\text{hot0}} = 1.3\,\%$. Figures 9(a) and 9(b) show the growth rate and frequency as a function of $\beta_{\text{thermal0}}$ for $q_0 = 0.80$ and $q_0 = 0.90$, respectively. It can be seen that both growth rate and frequency increase as $\beta_{\text{thermal0}}$ increases.
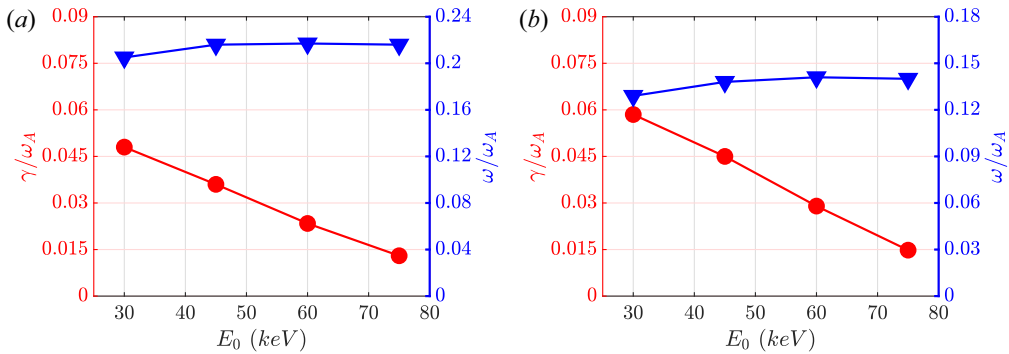
FIGURE 7. Growth rate and frequency dependence on $E_0$ for (*a*) $q_0 = 0.80$, (*b*) $q_0 = 0.90$.
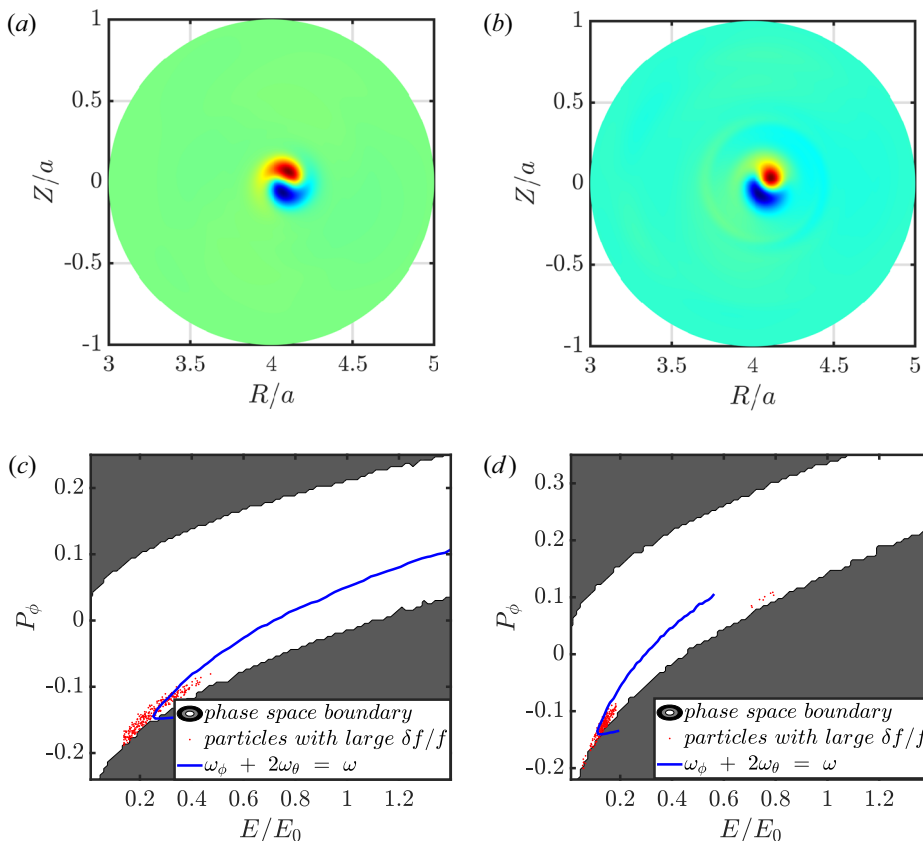


FIGURE 8. The mode structure (contour of $U$) of $q_0 = 0.80$ cases with (*a*) $E_0 = 30\,\text{keV}$ and (*b*) $E_0 = 75\,\text{keV}$; the resonance of $q_0 = 0.80$ cases with (*c*) $E_0 = 30\,\text{keV}$ and (*d*) $E_0 = 75\,\text{keV}$.

Figure 10 shows the continuum line of $m/n = 1/1$ for $q_0 = 0.80$ with several values of $\beta_{\text{thermal}0}$. The corresponding mode frequencies are also plotted in the figure. The results show that the continuum spectrum is up-shifted due to finite beta effects. In particular, the continuum frequency at the $q = 1$ surface is now finite. It can also be found that all the frequencies intersect with the corresponding continuum lines. Figure 11 shows the
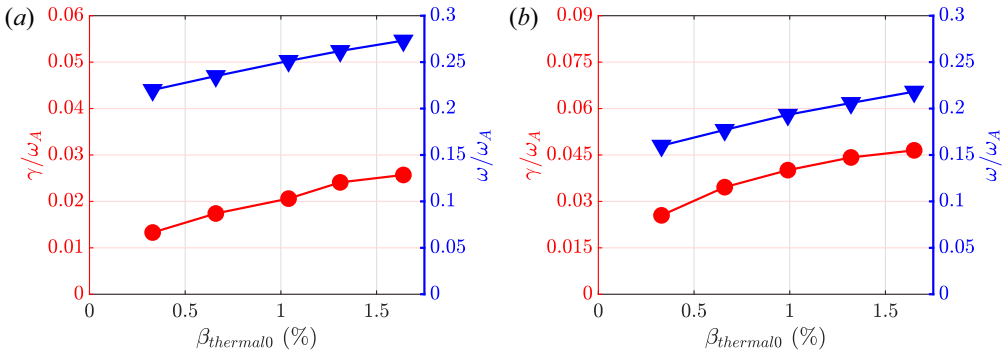
FIGURE 9. Growth rate and frequency dependence on $\beta_{\text{thermal0}}$ with (a) $q_0 = 0.80$,
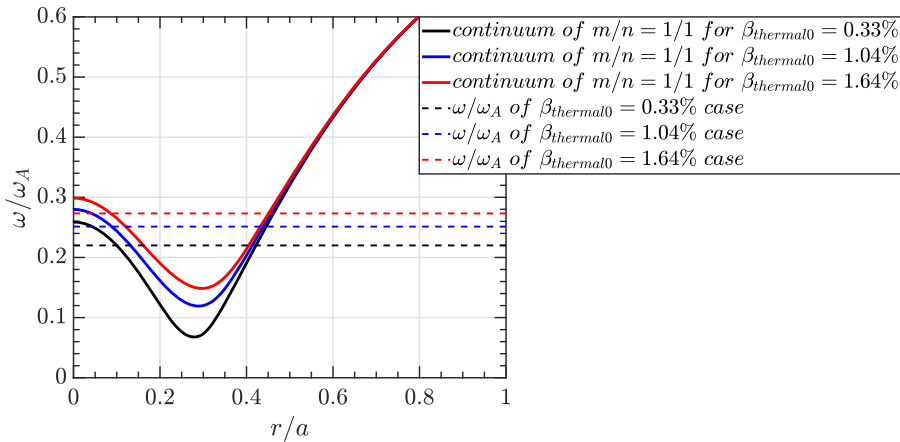(b) $q_0 = 0.90$.



FIGURE 10. Continuum spectrum and frequency of $q_0 = 0.80$ cases with different $\beta_{\text{thermal0}}$.

continuum lines of $m/n = 1/1$ and mode frequencies for $q_0 = 0.90$ with different $\beta_{\text{thermal0}}$. It can be found that all the frequencies are located above the tip of the continuum line at the magnetic axis. These results show that the mode type does not change as thermal beta varies. All the destabilized modes of $q_0 = 0.80$ cases are EPMs and all the modes of $q_0 = 0.90$ cases are GAEs. The main resonances of all these cases are still the same as the baseline case, i.e. $\omega_\phi + 2\omega_\theta = \omega$.

To summarize, the effects of finite thermal beta do not change the mode type, but they do have quantitative effects of increasing the mode frequency and growth rate for both EPM and GAE.

### 3.6. *Summary of linear simulation results*

In this section simulation results are presented for the energetic counter-passing beam ion-driven $n = 1$ mode in tokamak plasmas with monotonic $q$ profiles with $q_0 < 0$. The linear simulation results show that both EPMs and GAEs are destabilized by energetic particles via wave particle resonance of $\omega_\phi + 2\omega_\theta = \omega$ when the energetic particle beta exceeds a threshold value. The mode frequencies are of the order of $\omega/\omega_A \sim 0.2$, which is much higher than the typical frequency ($\omega/\omega_A \sim 0.04$) of the energetic co-passing particle-driven low-frequency fishbone (Yu *et al.* 2019) for similar parameters. The mode
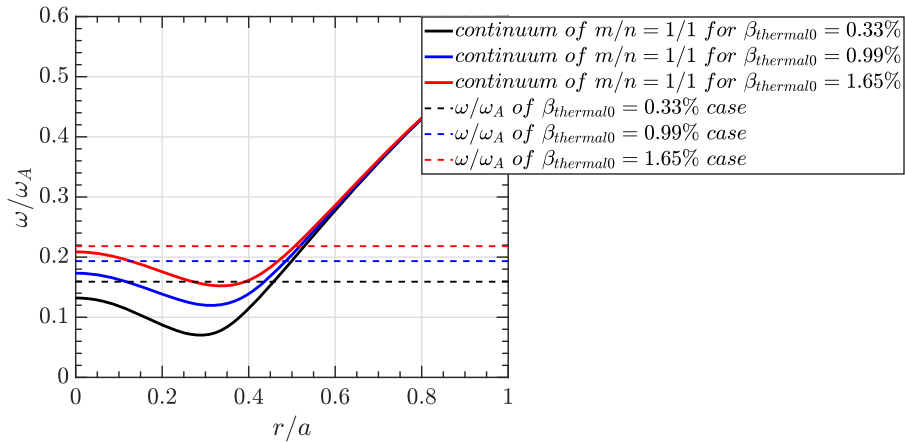
FIGURE 11. Continuum spectrum and frequency of $q_0 = 0.90$ cases with different $\beta_{\text{thermal}0}$.
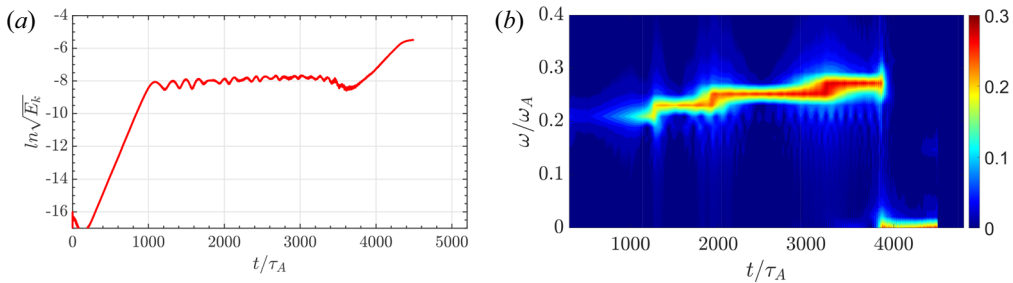


FIGURE 12. The evolution of kinetic energy and frequency.

structures are core localized within the $q = 1$ surface and are typically narrower than that of the internal kink mode or the low-frequency fishbone. Key parameter dependences are investigated. The results show that the instability is sensitive to the value of the central safety factor $q_0$. Both mode frequency and growth rate decrease as $q_0$ increases while the mode type transits from EPM to GAE as $q_0$ increases to $q_0 = 0.9$. For the dependence on beam ion injection energy $E_0$, it is found that mode frequency is not sensitive to $E_0$ while the growth rate decreases as $E_0$ increases. Finally, the simulation results show that the mode frequency and growth rate increase as the thermal plasma beta increases while the mode structure changes little.

## 4. Nonlinear simulation results of energetic counter-passing particle-driven modes

Here, we set $\beta_{\text{thermal}0} = 0.008\,\%$, $\beta_{\text{hot}0} = 0.96\,\%$, $q_0 = 0.80$ and $E_0 = 60\,\text{keV}$. Figure 12 shows the evolution of kinetic energy and mode frequency. As is shown in figure 12(a), the growth rate is approximately $0.11\omega_A$, and the mode saturates at approximately $1000\tau_A$. After a long period of nonlinear evolution at a nearly fixed amplitude, a new phase of mode growth appears at approximately $3600\tau_A$. From figure 12(b), at the first linear stage the mode frequency is approximately $0.21\omega_A$. The frequency chirps up to $0.27\omega_A$ during the nonlinear evolution before the second growth phase. At the beginning of the second growth phase, the mode frequency jumps down to a very low value.
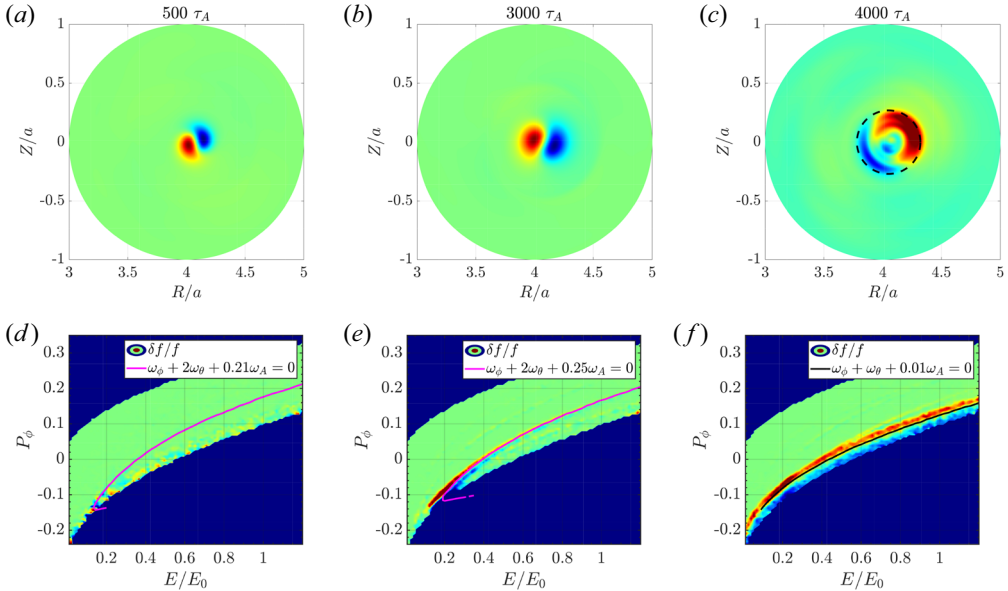
FIGURE 13. Mode structure (contour of $U$): (a) $t = 500\tau_A$, (b) $t = 3000\tau_A$, (c) $t = 4000\tau_A$. Resonance condition: (d) $t = 500\tau_A$, (e) $t = 3000\tau_A$, (f) $t = 4000\tau_A$.

In order to identify the types of the instabilities, we plot three mode structures at different times in figure 13(a–c). In figure 13(a), the mode structure corresponds to an EPM localized near the magnetic axis with $m/n = 1/1$ as the dominant harmonic in the first linear phase. In the nonlinear up-chirping phase, the mode structure becomes wider slightly. Finally, in figure 13(c) for the second growth phase, the mode changes to a low-frequency fishbone mode similar to the low-frequency mode driven by energetic co-passing particles found in our recent work (Yang *et al.* 2022).

To investigate the wave particle resonance condition, figure 13(d–f) plots contours of the normalized perturbed particle distribution $\delta f/f$ in phase space $(E, P_\phi)$ with $\Lambda = 0.02 \pm 0.02$ (i.e. integration of the particle distribution over these values of $\Lambda$) and the corresponding resonance lines at times of $500\tau_A$, $3000\tau_A$ and $4000\tau_A$, respectively. The resonance condition for the EPM is $\omega_\phi + 2\omega_\theta = \omega$. Energetic particles lie in the green area rather than the blue area of the phase space. For the low-frequency fishbone mode excited in the second growth phase, the resonance condition is $\omega_\phi + \omega_\theta = \omega$, which is the same as that of the co-passing energetic particle-driven low-frequency mode found previously (Yang *et al.* 2022).

We now consider the energetic particle transport during the nonlinear evolution. Figure 14 shows the evolution of energetic particle distribution $f(P_\phi)$ with pitch angle parameter $\Lambda = 0.02 \pm 0.02$ and normalized energies of (a) $E/E_0 = 0.19 \pm 0.01$ and (b) $E/E_0 = 0.7 \pm 0.01$ (i.e. integration of the particle distribution over these values of $\Lambda$ and $E$). During the nonlinear evolution phase, the energetic particles with $E/E_0 = 0.19 \mp 0.01$ have an obvious radial redistribution, as shown in figure 14(a). However, for particles with higher energies of $E/E_0 = 0.7 \pm 0.01$, there is little radial redistribution until the second growth phase after $t = 4000\tau_A$. Thus, later redistribution at higher energy is caused by the low-frequency mode excited during the second growth phase. This is consistent with the fact that the particle resonant energy of the low-frequency mode is much larger than that of the high-frequency EPM excited during the first growth phase.
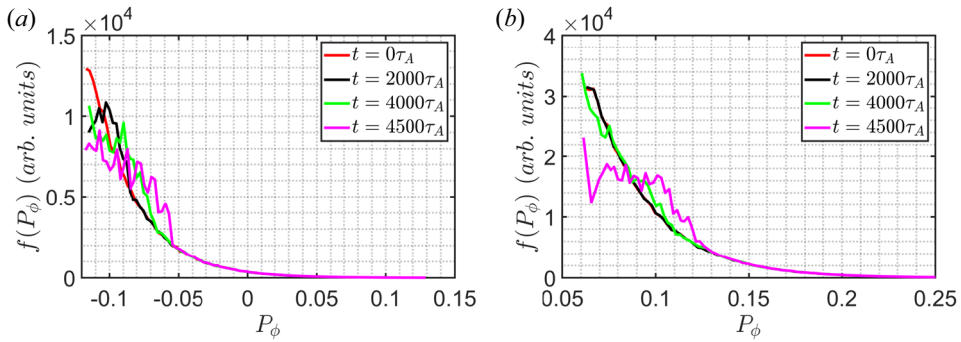
FIGURE 14. The redistribution of different resonant particles: (*a*) $E/E_0 = 0.19 \pm 0.01$, (*b*) $E/E_0 = 0.7 \pm 0.01$.
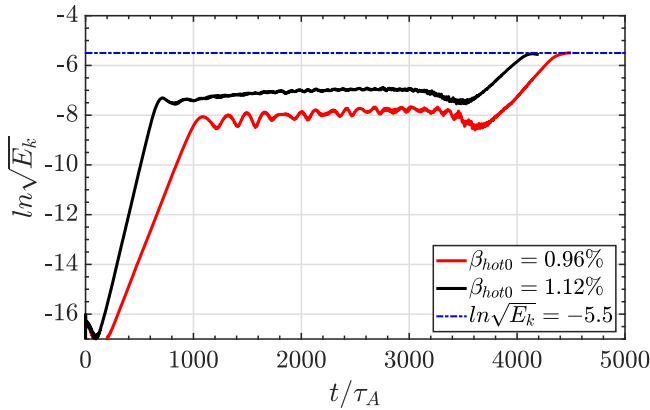


FIGURE 15. The kinetic energy evolution at different $\beta_{\text{hot0}}$.

Finally, we look at the effects of energetic particle beta on the nonlinear evolution of the instability. Figure 15 compares the kinetic evolution with two values of $\beta_{\text{hot0}}$. The red curve corresponds to the same case of $\beta_{\text{hot0}} = 0.96\,\%$ as presented in figure 12 while the black curve corresponds to the case with a slightly higher $\beta_{\text{hot0}}$. The higher beta case saturates earlier at a higher mode amplitude after the first growth phase. It also has a long quasi-steady saturation phase before the second growth phase. Overall, the features of nonlinear evolution of the higher beta case are very similar to those of the lower beta case.

## 5. Summary

A simulation study of the $n = 1$ instability driven by energetic counter-passing beam particles in tokamaks has been carried out using the kinetic-MHD hybrid code M3D-K. In the linear simulations, key parameters of the $q$ profile, beam ion beta and beam ion injection energy are scanned to investigate the dependence of linear mode properties on them. The results show that, depending on the value of the central safety factor $q_0$, the instability is either a $m/n = 1/1$ EPM or a $m/n = 1/1$ GAE destabilized by energetic particles. The main wave particle resonance responsible for driving the instability is found to be $\omega_\phi + 2\omega_\theta = \omega$. The mode frequencies are close to the tip of the Alfvén continuum spectrum at the magnetic axis and are much higher than that of the low-frequency fishbone

driven by energetic co-passing particles. These high-frequency modes are localized radially near the magnetic axis well within the $q = 1$ surface. Both the mode frequency and growth rate decrease as $q_0$ increases towards unity. The mode frequency is not sensitive to the beam injection energy while the growth rate decreases with increasing beam energy. Nonlinear simulations show that the mode saturates after the linear growth phase and has a long period of quasi-steady-state saturation with frequency chirping up. After this quasi-steady-state phase, the mode grows again while the frequency jumps down to a low value corresponding to a low-frequency fishbone. This low-frequency mode is similar to the low-frequency fishbone excited by energetic co-passing particles found previously (Yang *et al.* 2022). Correspondingly, the energetic particle distribution is flattened in the core of the plasma during nonlinear evolution, indicating a substantial re-distribution of energetic particles due to the instability. Finally, we suggest that an experiment be carried out to investigate energetic counter-passing beam ion-driven modes and to verify our results of GAE and EPM. Such an experiment could be done on HL-2A by reversing the direction of the plasma current.

## Declaration of interests

The authors report no conflict of interest.

## REFERENCES

APPERT, K., GRUBER, R., TROYUON, F. & VACLAVIK, J. 1982 Excitation of global eigenmodes of the alfven wave in tokamaks. *Plasma Phys.* **24** (9), 1147–1159.

BETTI, R. & FREIDBERG, J.P. 1993 Destabilization of the internal kink by energetic-circulating ions. *Phys. Rev. Lett.* **70**, 3428–3430.

CAI, H. & FU, G. 2012 Hybrid simulation of energetic particle effects on tearing modes in tokamak plasmas. *Phys. Plasmas* **19** (7), 072506.

CHEN, L. 1994 Theory of magnetohydrodynamic instabilities excited by energetic particles in tokamaks*. *Phys. Plasmas* **1** (5), 1519–1522.

CHEN, L., WHITE, R.B. & ROSENBLUTH, M.N. 1984 Excitation of internal kink modes by trapped energetic beam ions. *Phys. Rev. Lett.* **52**, 1122–1125.

CHEN, L. & ZONCA, F. 2016 Physics of alfvén waves and energetic particles in burning plasmas. *Rev. Mod. Phys.* **88**, 015008.

COPPI, B. & PORCELLI, F. 1986 Theoretical model of fishbone oscillations in magnetically confined plasmas. *Phys. Rev. Lett.* **57**, 2272–2275.

FU, G.Y., PARK, W., STRAUSS, H.R., BRESLAU, J., CHEN, J., JARDIN, S. & SUGIYAMA, L.E. 2006 Global hybrid simulations of energetic particle effects on the $n = 1$ mode in tokamaks: internal kink and fishbone instability. *Phys. Plasmas* **13** (5), 052517.

GORELENKOV, N.N., PINCHES, S.D. & TOI, K. 2014 Energetic particle physics in fusion research in preparation for burning plasma experiments. *Nucl. Fusion* **54** (12), 125001.

HEIDBRINK, W.W. 2008 Basic physics of alfvén instabilities driven by energetic particles in toroidally confined plasmas. *Phys. Plasmas* **15** (5), 055501.

LANG, J., FU, G.-Y. & CHEN, Y. 2010 Nonlinear simulation of toroidal alfvén eigenmode with source and sink. *Phys. Plasmas* **17** (4), 042309.

LIU, D., FU, G.Y., CROCKER, N.A., PODESTÀ, M., BRESLAU, J.A., FREDRICKSON, E.D. & KUBOTA, S. 2015 Hybrid simulation of toroidal alfvén eigenmode on the national spherical torus experiment. *Phys. Plasmas* **22** (4), 042509.

MAHAJAN, S.M., ROSS, D.W. & CHEN, G. 1983 Discrete alfvén eigenmode spectrum in magnetohydrodynamics. *Phys. Fluids* **26** (8), 2195–2199.

MCGUIRE, K., GOLDSTON, R., BELL, M., BITTER, M., BOL, K., BRAU, K., BUCHENAUER, D., CROWLEY, T., DAVIS, S., DYLLA, F., *et al.* 1983 Study of high-beta magnetohydrodynamic modes and fast-ion losses in pdx. *Phys. Rev. Lett.* **50**, 891–895.

PORCELLI, F., STANKIEWICZ, R., KERNER, W. & BERK, H.L. 1994 Solution of the drift-kinetic equation for global plasma modes and finite particle orbit widths. *Phys. Plasmas* **1** (3), 470–480.

SHEN, W., FU, G.Y., TOBIAS, B., VAN ZEELAND, M., WANG, F. & SHENG, Z.-M. 2015 Nonlinear hybrid simulation of internal kink with beam ion effects in DIII-D. *Phys. Plasmas* **22** (4), 042510.

SHEN, W., WANG, F., FU, G., XU, L., LI, G. & LIU, C. 2017 Hybrid simulation of fishbone instabilities in the EAST tokamak. *Nucl. Fusion* **57** (11), 116035.

WANG, F., FU, G.Y., BRESLAU, J.A. & LIU, J.Y. 2013 Linear stability and nonlinear dynamics of the fishbone mode in spherical tokamaks. *Phys. Plasmas* **20** (10), 102506.

WANG, S. 2001 Destabilization of internal kink modes at high frequency by energetic circulating ions. *Phys. Rev. Lett.* **86**, 5286–5288.

YANG, J., FU, G., SHEN, W. & YE, M. 2022 Linear hybrid simulations of low-frequency fishbone instability driven by energetic passing particles in tokamak plasmas. *Plasma Sci. Technol.* **24** (6), 065101.

YU, L., WANG, F., FU, G. & YU, L. 2019 Low-frequency fishbone driven by passing fast ions in tokamak plasmas. *Nucl. Fusion* **59** (8), 086016.

ZHU, X.L., WANG, F. & WANG, Z.X. 2020 Nonlinear simulation of multiple toroidal alfvén eigenmodes in tokamak plasmas. *Chin. Phys.* B **29** (2), 025201.